Electron Induced Modification of Self-Assembled Monolayers of Aromatic Carboxylic Acids

Andika Asyuda,[1] Rodrigo Ortiz de la Morena,[2] Eric Sauter,[1,§] Kelly Turner,[2] Kirsty McDonald,[2] Manfred Buck,[2,*] and Michael Zharnikov[1,*]

[1] *Angewandte Physikalische Chemie, Universität Heidelberg, Im Neuenheimer Feld 253, 69120 Heidelberg, Germany*

[2] *EaStCHEM School of Chemistry, University of St Andrews, North Haugh, St Andrews KY16 9ST, UK*

Abstract

The effects of low energy electrons on aromatic self-assembled monolayers (SAMs) with carboxylic acid (CA) docking groups were studied with focus on the dose range below 5 mC/cm^2. The SAMs were prepared on underpotentially deposited Ag bilayer and comprised non-substituted and CA-substituted monolayers with the rod-like biphenyl backbone and a monolayer of a Y-shaped, CA-substituted molecule, 1,3,5-benzenetribenzoic acid (H3BTB), formed either as a single-component film or as a binary one by mixing with adamantane-CA (Ad-CA). X-ray photoelectron and near-edge X-ray absorption fine structure spectra suggest a high proneness of the CA groups at both the SAM/substrate and SAM/ambient interface to electron irradiation. Cleavage of the carboxylate-substrate bond results in a substantial molecular desorption at the initial stage of irradiation until electron-induced cross-linking gradually takes over. The CA groups at the outer SAM interface undergo substantial chemical changes indicating that they participate in the cross-linking chemistry. The electron-induced processes are accompanied by molecular reorientation. Disordering concluded for the SAMs formed by the rod-like molecules is contrasted by the H3BTB based systems where changes also occur but some molecular order is preserved as explained by a proposed model invoking conformational changes. In SAMs of H3BTB mixed with Ad-CA the latter shows a higher proneness to irradiation-induced desorption than the former as well as an influence on the cross-linking chemistry. The results of the present study suggest that CA-based SAMs on Ag offer additional options for cross-linking in SAMs and, as exemplarily demonstrated by the generation of Cu patterns on structured H3BTB templates, can be efficiently used for lithography and nanofabrication.

1. Introduction

Compared to archetypical self-assembled monolayers (SAMs) with the thiolate docking group,[1,2] carboxylic-acid (CA) based SAMs, specifically those featuring aromatic backbones, have been investigated in detail only more recently.[3-15] These SAMs can be efficiently assembled from solution on a variety of substrates, including the coinage metals silver and copper. Silver, in particular, has turned out as beneficial for a flexible SAM design, owing to a comparatively weak interaction between the CA docking group and the substrate.[5-7,10,12,15] Consequently, the molecular structure and intermolecular interactions become factors for self-assembly dominating over molecule-substrate interactions, so that the structure and organization of a SAM can be flexibly tuned by design of its constituents. A variety of different arrangements was thus obtained, ranging from highly homogeneous, densely packed assemblies to layers featuring nanotunnels capable to store guest molecules.[7,10,15]

However, a particular feature of aromatic SAMs, viz. their reaction to electron irradiation, has hardly been addressed for CA-based systems.[16,17] In general, apart from pure scientific and e-beam/X-ray damage aspects,[18-20] electron irradiation of SAMs represents an important physical tool for the functionalization and patterning of surfaces. It was, in particular, used for creation of sophisticated mixed SAMs,[21,22] fabrication of chemical gradients,[23,24] fixation of metal films at the SAM-ambient interface,[25,26] work function tuning,[27] SAM-based lithography and related nanofabrication,[24,28-40] and preparation of SAM-based carbon nanomembranes (CNMs).[41-47] Such nanomembranes can, in general, be prepared from aromatic SAMs by relying on electron-induced cross-linking of the molecular backbones. CNMs fabricated from thiolate SAMs are, however, decorated with frequently undesirable, reactive thiol groups, stemming from the docking moieties of the parent monolayer and being of disadvantage for certain applications. However, as was demonstrated recently,[16] this problem can be avoided by the use of CA-based aromatic SAMs as the CNM precursor. As shown by the example of a densely packed, hybrid aliphatic-aromatic SAM, biphenyl-4-yl-ethane-CA (C_6H_5–C_6H_4–$(CH_2)_2$–COOH; termed as BP2-CA) on Ag(111) substrate, electron irradiation with a sufficiently high dose (150 mC/cm^2) results in efficient cross-linking of the aromatic part, accompanied by a nearly complete removal of the CA docking groups, giving, thus, an all-carbonaceous, chemically inert CNM after the transfer from the original support.[16] These findings are based on a combination of X-ray photoelectron spectroscopy (XPS) and scanning electron microscopy data, taken over the entire, quite extended (up to 150 mC/cm^2) dose range, with a particular emphasis on the high doses.

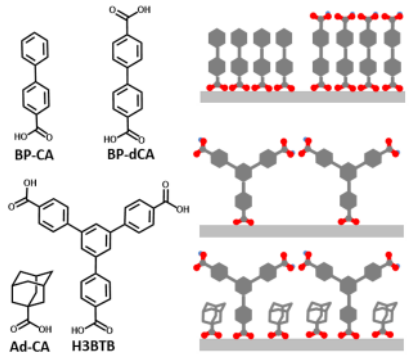

Figure 1. Molecular precursors of the present study, along with their acronyms. All molecules assemble in an upright configuration with one carboxylate moiety serving as docking group as illustrated by the cartoons on the right. H3BTB can form a SAM either on its own or with Ad-CA intercalated into its nanotunnels. For sake of simplicity, any inclination of molecules and differences in tilt angle between the systems have been omitted.

In this context, the present study specifically takes a look at the range of low doses, which is not only important for a deeper understanding of irradiation-induced processes in CA-based SAMs but can be potentially useful for fine modification of these films, as known for some of their thiol analogues.[27,48] As model systems, we look at a selection of aromatic SAMs with increasing complexity. The respective precursors, shown in Figure 1 together with illustrations of the corresponding SAM structures, comprise biphenyl-4-carboxylic acid (BP-CA),[7] biphenyl dicarboxylic acid (BP-dCA),[7] 1,3,5-benzenetribenzoic acid (H3BTB)[10] as well as a mixture of H3BTB and adamantane carboxylic acid (Ad-CA).[15] All these molecules form densely packed and well-structured SAMs on underpotentially deposited Ag(111), and bind to the substrate through a carboxylate moiety in a monopodal bidentate configuration.[7,10,15] BP-CA represents the basic reference system, with the rod-like biphenyl backbone adopting an upright orientation in the SAM. BP-dCA assembles similarly and the additional CA group should allow a comparison of the effect of electron irradiation on the carboxylate moiety at the SAM-substrate and the COOH group at the SAM-ambient interface. H3BTB has a Y-shape geometry. Notably, the molecules stack to rows which, in combination with the monopodal anchoring, results in a more open SAM structure[10] and, thus, enables the study of the effect of layer geometry on the irradiation behaviour. Finally, owing to the characteristic row structure of the H3BTB SAM, the combination of H3BTB and Ad-CA results in an interesting intercalation structure, with Ad-CA assembling within nanotunnels of the H3BTB layer, hardly interfering with the H3BTB arrangement.[15] Such a bicomponent layer, where aliphatic and aromatic compounds are mixed in a well defined way, represents a model

system to monitor the effect of admixture on irradiation-induced behaviour; in the present case, to test for differences to the pure H3BTB layer.

Generally, the behavior of SAMs upon electron irradiation represents a superposition of several simultaneously running processes, such as molecular decomposition, desorption of the SAM forming molecules and their fragments, progressing disordering, damage of the SAM/substrate and SAM/ambient interfaces, and chemical reactions in the residual SAM matrix, including cross-linking between individual molecules and their skeletons.[18] The exact kinetics and relative weight of these processes depend on molecular structure, packing density and structural perfection of a SAM, as well as the character of the substrate.[18] An established powerful way to monitor these processes is a combination of XPS and X-ray absorption spectroscopy as information on changes in both chemical composition and orientational order is obtained.[25,28,39] Accordingly, this combination was also applied here as the major experimental tool, complemented by selected additional experiments employing scanning tunneling microscopy (STM).

2. Experimental

$AgNO_3$ (99.9999%, Sigma-Aldrich), ethanol (AnalaR Normapur), H3BTB (99%, Sigma-Aldrich) and Ad-CA (99%, Sigma-Aldrich) were used as purchased. Biphenyl-4-carboxylic acid (95%, Sigma-Aldrich) and biphenyl-4,4'-dicarboxylic acid (97%, Sigma-Aldrich) were recrystallized from ethanol prior to use. Au substrates (300 nm epitaxial Au(111) layer on mica, Georg Albert PVD, Silz, Germany) were annealed using a natural gas flame before underpotential deposition (UPD) of a (1×1) Ag bilayer was carried out. For this purpose, Au/mica was immersed in 10 mM $AgNO_3$ in 100 mM HNO_3 (aq) and a potential of 10 mV (vs. Ag/Ag^+) was applied to the substrate for 2 minutes. This yields full coverage of a stable bilayer of silver atoms.

The SAMs were prepared according to established procedures; see ref. 7 for BP-CA and BP-dCA, ref. 10 for H3BTB, and ref. 15 for H3BTB/Ad-CA. The binary SAM was prepared by sequential adsorption of H3BTB and Ad-CA, also resulting in the highly regular row structure of the native H3BTB layer but with the Ad-CA molecules assembled in the nanotunnels of the H3BTB structure.[15]

All experiments were performed at room temperature. The electron irradiation was carried out in a step-like fashion, with a Leyboldt-Heraeus FG 15/40 flood gun (50-500 eV). The energy of electrons was set to 50 eV. The electron flux was calibrated by a Faraday cup; the

maximum dose was 4 mC/cm^2. The electron gun was mounted at a distance of 10-15 cm from the sample to ensure uniform illumination. The base pressure during irradiation was 1×10^{-8} mbar. Note that the kinetics of the irradiation-induced processes generally depends on the electron energy[46,47,49-52] but 50 eV is a good choice in this context since it is frequently used for SAM modification[27,46] and was in particular used in the recent study of CA-based SAM,[16] so that the respective results can be directly compared with the presented data.

The modification of the SAMs upon exposure to electrons was monitored by synchrotron-based XPS and near-edge X-ray absorption fine structure (NEXAFS) spectroscopy. The characterization was performed both *in situ*, immediately after each irradiation step. The measurements were performed at the HE-SGM beamline (bending magnet) of the synchrotron storage ring BESSY II in Berlin, Germany, using a custom-made experimental station equipped with a Scienta R3000 electron energy analyzer.[53]

The acquisition of the XP spectra, for the Au 4f, Ag 3d, C 1s, and O 1s ranges, was carried out in normal emission geometry at an excitation energy of 580 eV. This energy was selected as a compromise between the energy resolution (~0.5 eV) and sufficiently high photon flux. The binding energy (BE) scale of the XP spectra was referenced to the Au $4f_{7/2}$ emission at 84.0 eV.[54] The spectra were fitted by symmetric Voigt functions and a linear background using CASA-XPS software. The derived intensities were in particular used for the calculation of the effective thickness of the SAMs, based on the C 1s/Ag 4d and C 1s/Au 4f intensity ratios (the total C 1s intensity was considered) and taken the thicknesses of the pristine monolayers, known from the previous work,[7,10,15] as the reference.[55] A standard expression for the attenuation of the photoemission signal was assumed[56] and the literature values for attenuation lengths were used.[57]

The NEXAFS spectra were collected at the C K-edge in a partial electron yield mode. The retarding voltage was set to −150 V. The primary X-ray light was linearly polarized with a polarization factor of ca. 90%. The energy resolution was ca. 0.3 eV. The incident geometry of the X-ray light was varied from the normal to grazing incidence in steps of 10–20° to monitor orientational order in the SAMs. This approach is based on the strong dependence of the cross-section of the resonant photoexcitation process on the orientation of the electric field vector of the linearly polarized light with respect to the molecular orbital of interest, termed as linear dichroism in X-ray absorption.[58] The photon energy scale was referenced to the pronounced π^* resonance of highly oriented pyrolytic graphite at 285.38 eV.[59] The spectra were corrected for the photon energy dependence of the photon flux and reduced to the

standard form, with the zero signal in the pre-edge region and the unity edge jump in the far post-edge region.

The above experiments were complemented by laboratory measurements performed for the H3BTB SAM only, over a dose range of 0-150 mC/cm^2. The samples were homogeneously irradiated with a flood gun (FG20, Specs, Germany), at a base pressure better than 1×10^{-8} mbar. The electron energy was set to 50 eV and the dose was calibrated by an array of Faraday cups. The effect of irradiation was monitored *in situ* by XPS. The measurements were carried out with a MAX200 (Leybold-Heraeus) spectrometer equipped with an Mg Kα X-ray source (200 W) and a hemispherical analyzer. Normal emission geometry was used.

The pristine and irradiated H3BTB samples were additionally characterized by scanning tunneling microscopy (STM). The characterization was performed *ex situ*, after exposure of the samples to ambient and a few days storage necessary for the sample delivery between labs. STM imaging was carried out using a Molecular Imaging PicoSPM system in ambient atmosphere. Tips were mechanically cut from Pt/Ir 80 : 20 wire (Advent Research Materials Ltd, 0.25 mm diameter). Tunneling current and tip bias were in the range of 2–70 pA and ±0.20–0.60 V.

Finally, to visualize the effect of electron irradiation and to test the efficiency of cross-linking for aromatic molecules with Y-shape geometry, we performed the electrochemical deposition of Cu on H3BTB-based templates, patterned in proximity printing geometry using an R2/4 Quantifoil® as mask and 300 eV electrons with a dose of ca. 100 mC/cm^2. Note that the efficiency of 300 eV electrons in context of cross-linking is higher by a factor of ca. 1.5 as compared to 50 eV electrons.[46] The electrochemical deposition of Cu was performed in an acidic 50 mM $CuSO_4$ electrolyte applying a potential of -0.3 V (vs Cu^{2+}/Cu). The fabricated patterns were imaged with an atomic force microscope (AFM, Nanosurf EasyScan 2) in contact mode using a silicon cantilever (Budget Sensors ContAl-G, k = 0.2 N/m) and a setpoint of 42 nN.

3. Results

3. 1. General Spectroscopic Data

The pristine BP-CA, BP-dCA, H3BTB, and H3BTB/Ad-CA SAMs on UPD-Ag have been described in detail previously.[7,10,15] In short, the structure of the BP-CA SAM is characterized by a rectangular ($5 \times \sqrt{3}$) unit cell for the prevailing phase, corresponding to a molecular area

of 24 Å^2 and molecular inclination of about 10°.[7] The structure of the BP-dCA SAM is described by an oblique ($\sqrt{93} \times \sqrt{133}$) unit cell, corresponding to a molecular area of 26.5 Å^2. The bonding to the substrate is mediated by one of the two CA groups and the average molecular inclination was determined to ~25°.[7] H3BTB, also anchored to the substrate via one CA group, forms a distinct row structure with the molecules inclined along the rows by ca. 30°. The molecular packing arises from π-stacking of the molecules and interrow hydrogen bonding of the other two COOH groups.[10] Described by a $\sqrt{7} \times \sqrt{31}$ unit cell, the molecular area of 61.5 Å^2 is significantly larger compared to the other systems. This is a consequence of the Y-shaped geometry of H3BTB which, therefore, gives rise to an open SAM structure featuring nanotunnels as indicated in Figure 1. The H3BTB/Ad-CA SAM, prepared by the sequential deposition of H3BTB and Ad-CA, is homologous to that of the single-component H3BTB monolayer, with Ad-CA molecules intercalated in the nanotunnels of the H3BTB layer.[15]

The quality and high structural order of the pristine SAMs of BP-CA, BP-dCA, H3BTB, and H3BTB/Ad-CA was verified in the present work with XP and NEXAFS spectra, and STM images also serving as reference to monitor the effect of electron irradiation.

Representative XPS and NEXAFS data for the BP-CA SAM are presented in Figure 2. The C 1s XP spectrum of the pristine SAM in Figure 2a exhibits a strong peak at 284.1 eV and a weak peak at 287.2 eV assigned to the biphenyl backbone and the CA docking group, respectively.[7] The respective O 1s XP spectrum in Figure 2b shows a single peak at 530.2 eV, which reflects the presence of the CA group as carboxylate and binding to the substrate in a bidentate configuration.[7] The most salient feature in the 55° C K-edge spectrum of the pristine BP-CA SAM in Figure 2c is the π^*_{ph} resonance at 285.0 eV from the biphenyl backbone.[48,60-62] The other significant resonance of interest here comes from the CA group, represented by a π^*_{CA} resonance at 288.3 eV.[7] This "magic angle" spectrum is exclusively representative of the electronic structure of the SAM and is not affected by orientational effects.[58] In contrast, the difference spectrum of the pristine BP-CA SAM in Figure 2d is characteristic of molecular orientation in the film, emphasized by the difference peaks at the positions of the characteristic absorption resonances.[58] The distinctly positive sign of these peaks for the π* resonances reflects the upright molecular orientation.[7]

Electron irradiation results in progressive decrease of both C 1s peaks (Figure 2a). Along with the increase of the Ag 3d and Au 4f intensities (not shown), this suggests a reduction in film thickness and modification/loss of CA groups at the SAM/substrate interface. Interestingly,

the shape of the 55° NEXAFS spectra does not change much, except for a decrease in the relative intensity of the π^*_{CA} resonance (Figure 2c), which, along with the C 1s XP data, means that (i) the thickness reduction is predominantly mediated by desorption of entire molecules and not by fragments and (ii) the modification of the SAM/substrate interface occurs faster than desorption. The latter statement is supported by the rapid evolution of the O 1s XP spectra (Figure 2b), which will be further substantiated below. The electron-induced modification of the SAM is accompanied by the loss of orientational order, as follows from the significant decrease in the amplitude of the characteristic difference peaks in the 90°-20° NEXAFS spectra (Figure 2d). However, the order is not destroyed completely, since the dichroism is still observed at the highest dose of our experiments.

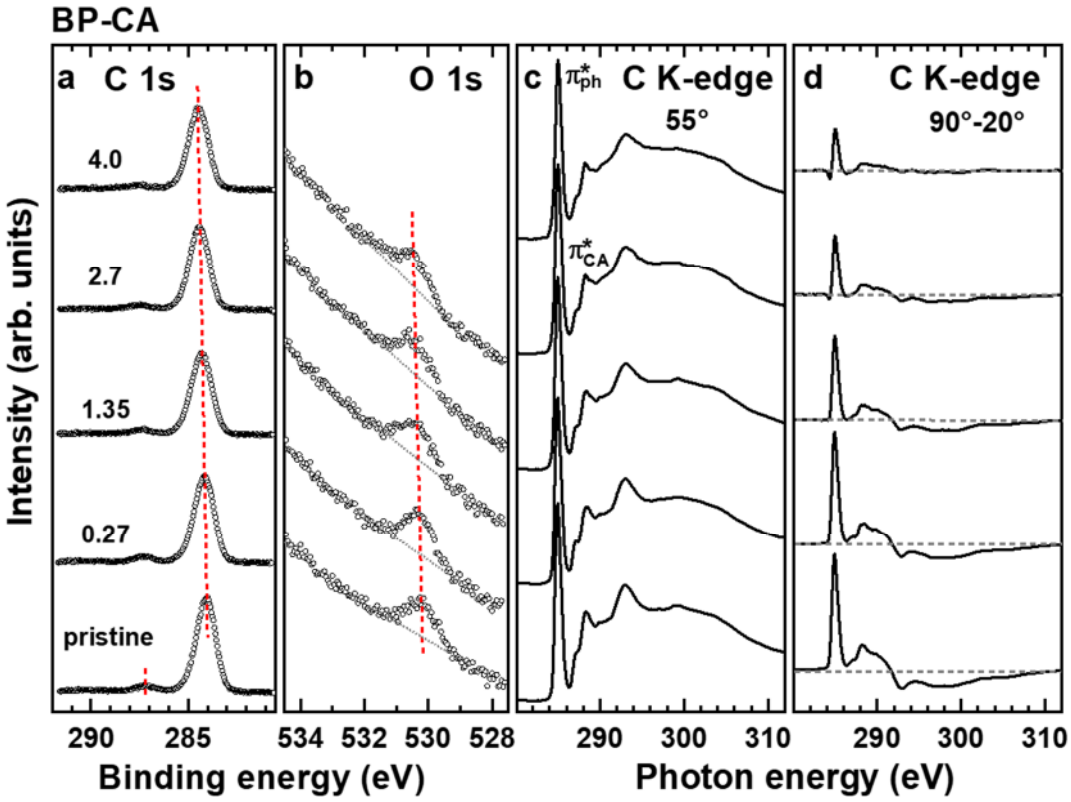

Figure 2. Spectroscopic data for the pristine and irradiated BP-CA SAM: C 1s (a) and O 1s (b) XP spectra, C K-edge NEXAFS spectra acquired at an incidence angle of 55° (c), and the difference between the NEXAFS spectra acquired at incidence angles of 90° and 20° (d). Irradiation doses (in mC/cm^2) corresponding to the individual spectra are indicated in panel a. The maxima of the C 1s and O 1s signals are traced by red dashed lines. The additional mark in the C 1s spectrum of the pristine SAM denotes the COO^- signal (~287.2 eV). Dashed black lines in panels b and d mark baselines and zero lines, respectively.

The XP and NEXAFS spectra of the pristine BP-dCA and H3BTB SAMs are similar to each other, which is understandable since for both molecules one CA group is present as carboxylate and bound to the substrate whereas the other one(s) is/are located at the SAM-ambient interface.[7,10] Since also the electron-induced changes in the spectra exhibit parallels (apart from the anisotropy in the NEXAFS spectra, see below), we only present data for the H3BTB SAMs here (Figure 3) and refer to Supporting Information for the corresponding series of spectra of BP-dCA (Figure S1). However, we note at this point that there are significant quantitative differences between the two SAMs and these will be discussed below.
The presence of unbound CA groups in the pristine BP-dCA and H3BTB SAMs gives rise to some difference in the spectra compared to BP-CA. First, there is the additional, low intensity peak at 288.9 eV in the C 1s XP spectrum of the COOH group/groups at the SAM-ambient interface (Figure 3a). Second, the O 1s spectra are dominated by the C–OH and C=O signals in the range of 531-534 eV (Figures 3b and S1b). Third, the π^*_{CA} resonance, to which both the COO^- and COOH groups contribute, is much more pronounced than in the BP-CA case (Figure 3c) and exhibits a stronger dichroism (Figure 3c), especially for the BP-dCA SAM (Figure S1d). Reasons are the stronger attenuation of the signal from the buried carboxylate moiety compared to the COOH located at the outer SAM interface,[63] and the mixing of states of the carboxylate moiety and the substrate, thus, affecting oscillator strength and, to some extent, orientation of the transition dipole moment.

The C 1s XP and 55° NEXAFS spectra of the irradiated BP-dCA and H3BTB SAMs, along with the respective increase of the Au 4f and Ag 3d substrate signals (not shown), display dose dependent trends similar to that of the BP-CA monolayer, again suggesting, (i) a progressive thickness reduction, predominantly caused by desorption of entire molecules and (ii) a damage of the SAM/substrate and SAM/ambient interface occurring simultaneously with desorption. Notably, there are distinct differences in the change of orientation between the BP-dCA and H3BTB SAMs, reflected in the NEXAFS difference spectra. In the former case, the amplitude of the characteristic peaks in the 90°-20° spectra progressively decreases well beyond what is observed for BP-CA and approaching zero at the maximum dose of our experiments, suggesting a nearly complete disordering of the monolayer. In the latter case, the anisotropy signal first also decreases and then, in remarkable contrast to both BP-CA and BP-dCA, increases again but with the sign inverted. As discussed in detail in Sec. 4, this indicates an irradiation-driven reorientation of the H3BTB moieties rather than a disordering. It is a very unusual phenomenon which, in a different form but also at low doses, has, so far, only been observed for the monolayer of 1,1'-biphenyl-4-thiol on Au(111).[48]

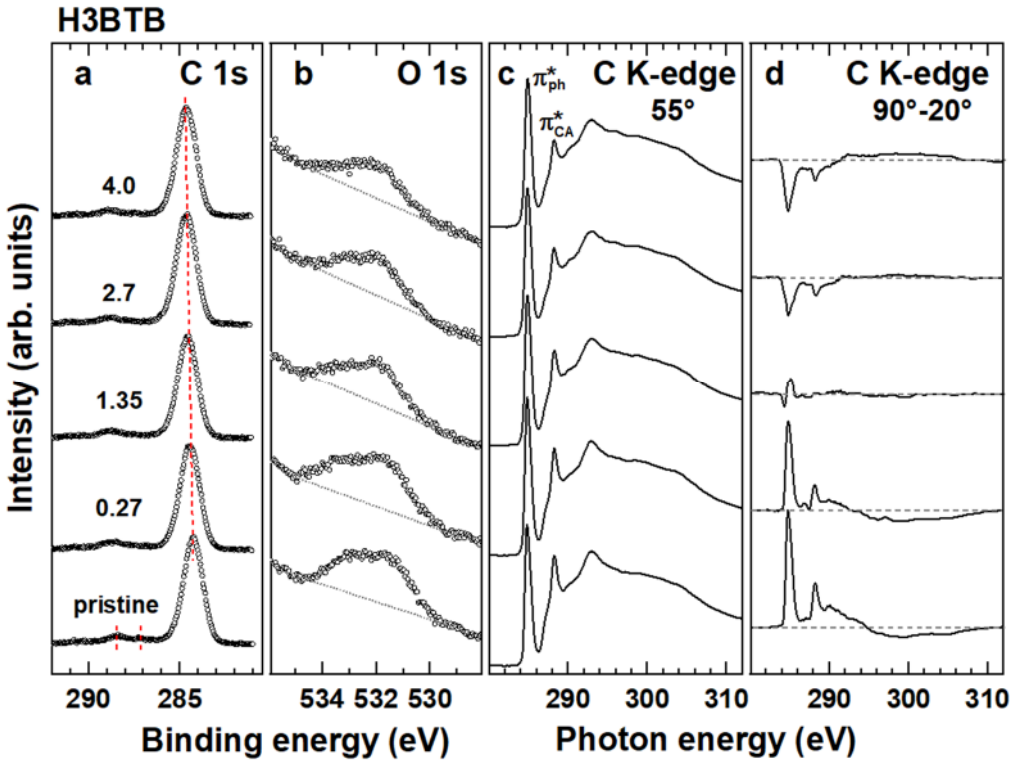

Figure 3. Spectroscopic data for the pristine and irradiated H3BTB SAM: C 1s (a) and O 1s (b) XP spectra, C K-edge NEXAFS spectra acquired at an incidence angle of 55° (c), and the difference between the NEXAFS spectra acquired at incidence angles of 90° and 20° (d). Irradiation doses (in mC/cm^2) corresponding to the individual spectra are indicated in panel a. The maxima of the C 1s signals are traced by the red dashed line. The additional marks in the C 1s spectrum of the pristine SAM denote the COO^- (~287.1 eV) and COOH (~288.5 eV) signals. Dashed black lines in panels b and d mark baselines and zero lines, respectively.

As to the binary SAM of H3BTB and Ad-CA, the XP and NEXAFS spectra (Figure S2) of this system are quite similar to those of the pure H3BTB monolayer (Figure 3), both for the pristine films and in the course of irradiation. Significantly, the presence of the adamantane compound does not fundamentally affect the reorientation of the H3BTB molecules as the inversion of the anisotropy signal in the NEXAFS difference spectra (Figure S2d) is also observed for the binary SAM.

3.2. O 1s XP Spectra

The O 1s XP spectra of the SAMs, only briefly touched upon above, exhibit significant changes with electron dose. In view of the primary role of the CA groups in bonding to the substrate (COO^-) and molecular assembly (COOH) a quantitative analysis was performed by

fitting the background-corrected spectra. The results for the pristine and irradiated (4 mC/cm^2) SAMs of all investigated systems are shown in Figure 4. Over the energy range of the O 1s signal a linear background was used as indicated by the dashed lines in Figures 2, 3, S1, and S2. The spectra of the native SAMs with COOH groups were fitted by fixing the C–OH and C=O signals to the stoichiometric 1:1 ratio. This restriction was lifted when fitting the spectra of the irradiated samples. Furthermore, since the signal from the carboxylate moiety at the SAM/substrate interface is small compared to the COOH signal due to the substantial attenuation of the electrons, the position of the carboxylate signal and its line width were restricted to ensure a consistent fit.

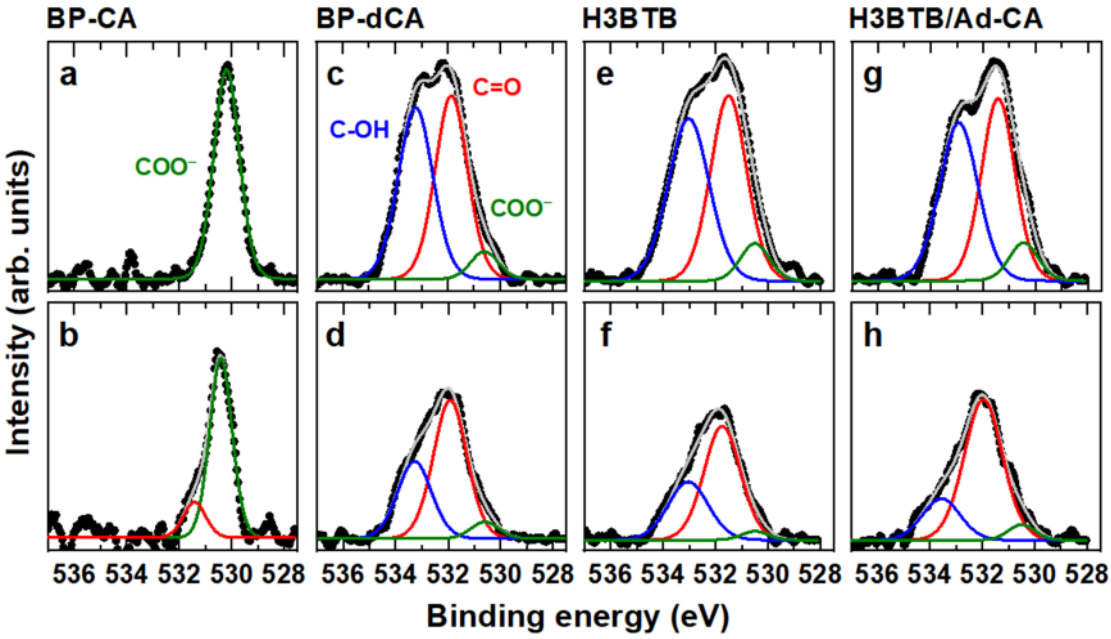

Figure 4. Background-corrected O 1s XP spectra of the pristine (upper row) and irradiated (4 mC/cm^2; bottom row) SAMs of BP-CA (a,b), BP-dCA (b,c), H3BTB (e,f), and H3BTB/Ad-CA (g,h). The experimental spectra (black circles) are decomposed into individual peaks with C**OO**$^-$ (green), C=**O** (red) and C–**O**H (blue) components and the envelope (gray) colour coded. The spectra of the pristine SAMs are normalized to the maximum intensity. Intensities of the spectra of the irradiated SAMs are relative to the respective pristine monolayers.

As mentioned above, the spectrum of the pristine BP-CA SAM (Figure 4a) exhibits the signal of the carboxylate docking group at 530.4 eV.[7] Upon electron irradiation its intensity decreases slightly and an additional feature characteristic of a C=O group emerges at ca. 531.4 eV (Figure 4b). Furthermore, it is described by a line profile which exhibits the same

linewidth as the main component. Lacking a broad wing towards higher BEs the shape is different to irradiated BP2-CA SAMs recently reported in the literature[16] (see also Sec. 1) and we will return to this point in Sec. 4. The changes in the docking group are paralleled by a progressive upward shift of the photoemission peaks which is interpreted to be an electrostatic effect[64,65] as a consequence of charge rearrangement at the SAM/substrate interface. This behavior, reported for the BP2-CA SAMs before,[16] is specifically traced in the C 1s XP spectra. For the BP-CA SAM (Figure 2a) the shift of the major C 1s peak at a dose of 4 mC/cm^2 amounts to 0.5 eV, with similar values also observed for the other systems (see Figures 3a, S1a, and S2a).

The O 1s XP spectra of the pristine SAMs of BP-dCA (Figure 4c), H3BTB (Figure 4e), and H3BTB/Ad-CA (Figure 4g) can be decomposed into three components at ~530.5 eV, ~531.8 eV, and ~533.2 eV corresponding to the COO^- docking group, and the C=O and C–OH contributions of the unbound COOH groups, respectively.[7,10,15] As expected from the chemical composition (Figure 1) and the upright monopodal adsorption geometry, the signal from the buried COO^- moiety is attenuated and, thus, small compared to the intensities of the C=O and C–OH peaks, which are well described by the expected, stoichiometric 1:1 ratio, albeit their line widths are slightly different.

Electron irradiation results in an intensity decrease for all three components but their evolution varies substantially with the systems as evidenced by Figures 4d, 4f and 4h. The most salient features are the significant reduction in the signal intensities and the distinct change in the shape of the spectra, which is phenomenologically described by the change in the intensity ratio of the C=O and C–OH components. It appears that the COOH moieties undergo chemical changes to a significant extent and are involved in the cross-linking chemistry, in addition to their desorption as complete entities. This is corroborated by a study of a COOH terminated aliphatic thiolate SAM where low energy electrons were observed to trigger the emission of CO species from a layer of 11-mercaptoundecanoic acid.[66] As to electron-induced changes in the C=O/C–OH ratio, the extent to which this occurs is system dependent. BP-dCA and H3BTB behave rather similarly with the C=O/C–OH ratio increasing from 1 of the native SAMs to about 1.8 at a dose of 4 mC/cm^2, which is somewhat surprising, given the rather different location and orientation of the COOH groups in the two SAMs. For the mixed H3BTB/Ad-CA SAM this ratio is significantly higher (~3.4) which suggests that Ad-CA is affecting the irradiation induced chemistry.

Concluding this section, we stress that in the analysis of the spectra presented in Figure 4 a simplistic approach was taken to get a grip on the radiation-induced changes by employing a consistent fitting scheme to all spectra. While the changes in the spectral components give clear evidence of chemical reactions involving the COOH groups, there is a range of functionalities comprising esters, aldehydes, ketones, alcohols, or ethers whose O 1s signatures are spread across the 531-534 eV range.[67] Therefore, with detailed information on chemical functionalities in the cross-linked SAMs lacking at present, the two component description of the range represents a phenomenological approach rather than a reflection of the details of the chemistry. Consequently only the sum of the C=O and C–OH signals is strictly meaningful for a quantitative assessment and comparison of the spectra as presented in the next section.

3.3. Comparison of Individual SAMs

The behavior of the CA-based SAMs can be compared in more detail by analysis and comparison of the most relevant parameters. The XPS-derived parameters are compiled in Figure 5 with the reference values of the effective thicknesses calculated on the basis of the molecular length, length of the CA-Ag bond, and molecular tilt.[7,10,15] The effective thickness of all SAMs in Figure 5a decreases with increasing dose, showing a similar behavior for the BP-CA, BP-dCA and H3BTB SAMs and a noticeably larger decrease for the H3BTB/Ad-CA monolayer. For the former three SAMs the thickness decreases by 25-30% at a dose of 4 mC/cm^2. Such a relatively large reduction in thickness, which is significantly larger compared to thiol SAMs (≤10%)[46,68] and also reported for BP2-CA(~28%),[16] is related to the irradiation induced processes at the SAM-substrate interface and points to the desorption of entire molecules before cross-linking in the SAM takes over. We note at this point that film thickness reflects the amount of material present. Therefore, it should not be interpreted as a geometrical thickness, in particular when comparing SAMs with different structures, but rather be understood as an indicator of loss of material.

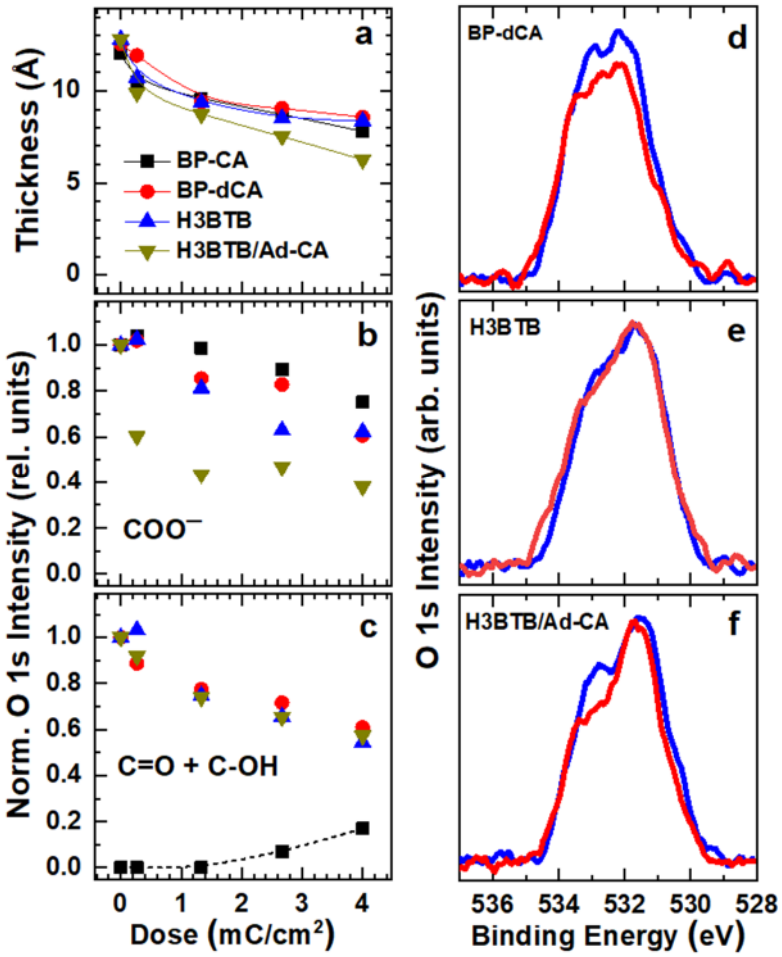

Figure 5. Left panels (a-c): Thickness (a) and O 1s XP signals (b, c) of the CA-based SAMs as functions of irradiation dose. The O 1s components, normalized to the values for the pristine SAMs, are separated into the carboxylate signal (b) and the sum of the C–OH and C=O signals (c). The intensity of the second component in the BP-CA O 1s spectra (black squares in panel c is normalized to that of the COO^- signal of the pristine layer at the respective dose. For legend to symbols see panel a. As a guide to the eye some of the data sets are connected by solid or dashed lines. The accuracy of the values is ±5%, except for the COO^- signal of BP-dCA, H3BTB and H3BTB/Ad-CA (for explanation, see text). Right panels (d-e): Comparison of the O 1s XP spectra of the native (blue curves) and irradiated (0.27 mC/cm^2; red curves) SAMs for BP-dCA (d), H3BTB (e), and H3BTB/Ad-CA (f).

The effective thickness of the H3BTB/Ad-CA monolayer decreases even more than for the other SAMs. This can only be related to the comparatively high proneness of Ad-CA to irradiation-induced desorption, which is confirmed by the dose dependent behavior of the normalized O 1s (COO^-) and O 1s (COOH) intensities in Figures 5b and 5c, respectively. Whereas the O 1s (COO^-) intensity in the mixed SAM, which is determined by both H3BTB

and Ad-CA, decreases more compared to the pure H3BTB monolayer, the O 1s (COOH) intensity, which is only related to H3BTB, behaves essentially identical for the H3BTB/Ad-CA and H3BTB SAMs. Apart from the above mentioned difference, the O 1s (COO^-) intensity for all CA-based SAMs of the present study decreases progressively upon irradiation, showing no saturation in the energy range investigated (Figure 5b). The decrease in the amount is even larger than Figure 5b implies, since the O 1s (COO^-) signal from the SAM-substrate interface is less attenuated with progressive irradiation due to the reduction in film thickness. Consequently, the O 1s (COO^-) intensity drop of 25-40%, observed for the BP-CA, BP-dCA and H3BTB SAMs at a dose of 4 mC/cm^2, corresponds likely to a density reduction of 37-60% for the oxygen atoms in the COO^- docking groups, which is a fairly high amount for such a comparably small dose. We would like to point here that the scattering of the carboxylate intensity data in Figure 5b for all systems but BP-CA is larger compared to the COOH data in Figure 5c because, as seen from Figure 4, the carboxylate signals of the former are rather small compared to the other two signals and, therefore, are subject of a larger uncertainty within the fitting process. From variations in the constraints of fitting parameters the error in the COO^- is estimated to about 15%. This restricts the interpretation of the data to the difference between the mixed and pure H3BTB based SAMs whereas, at this point, potential differences between the monocomponent systems are not sufficiently clear cut. Measurements at higher photon energies causing less attenuation of the carboxylate signal could provide further insight .

For BP-CA the progressive decrease of the O 1s (COO^-) signal is accompanied by the emergence of a C=O signal at ~531.4 eV (Figure 5c, black squares) as already pointed out above (Figure 4b). It becomes significant above 1.35 mC/cm^2 and reaches a value of about 20% of the carboxylate signal at the highest dose of 4 mC/cm^2.

The total O 1s signal of the terminal CA groups, i.e., the sum of the C=O and C–OH components, exhibits a nearly identical decrease for the BP-dCA, H3BTB and H3BTB/Ad-CA. Whereas this suggests that neither the molecular geometry of the aromatic molecules (rod-like vs. Y-shaped) nor the presence of additional small molecules like Ad-CA significantly affect the sensitivity of these groups to electron irradiation, some differences between the systems are discernible as seen from panels d-f of Figure 5, which compare the spectra of the SAMs before and after irradiation at low dose. For BP-dCA (Figure 5d) with the outward pointing COOH group, both the C=O and C–OH components decrease which suggests the loss of entire COOH groups, either due to molecular fragmentation or loss of the

entire molecules. For H3BTB (Figure 5e) changes are very subtle and it is impossible to decide without further analysis, e.g. by vibrational spectroscopy, whether this indicates an onset of chemical changes or just changes in molecular orientation and supramolecular interactions between COOH moieties. For the mixed H3BTB/Ad-CA SAM there is again a clear change. However, in contrast to BP-dCA, the C–OH component at ~533 eV is more affected than the C=O region (~531.5 eV), thus pointing to chemical changes different from a mere loss of COOH groups and, thus, a significant influence of Ad-CA which desorbs to a significant extent at the lowest dose as seen from the change in the carboxylate signal in Figure 5b. It is noted that the differences in the COOH region between the systems are only noticeable at the lowest dose of our experiments. At higher doses more substantial changes occur across the whole spectral range as exemplified by the 4 mC/cm^2 spectra in Figures 4d-f. These changes arise from fragmentation and chemical processes associated with the cross-linking; thus accounting for a loss of ~40% of the COOH signal (Figure 5b) and a 30-50% reduction in film thickness at this dose.

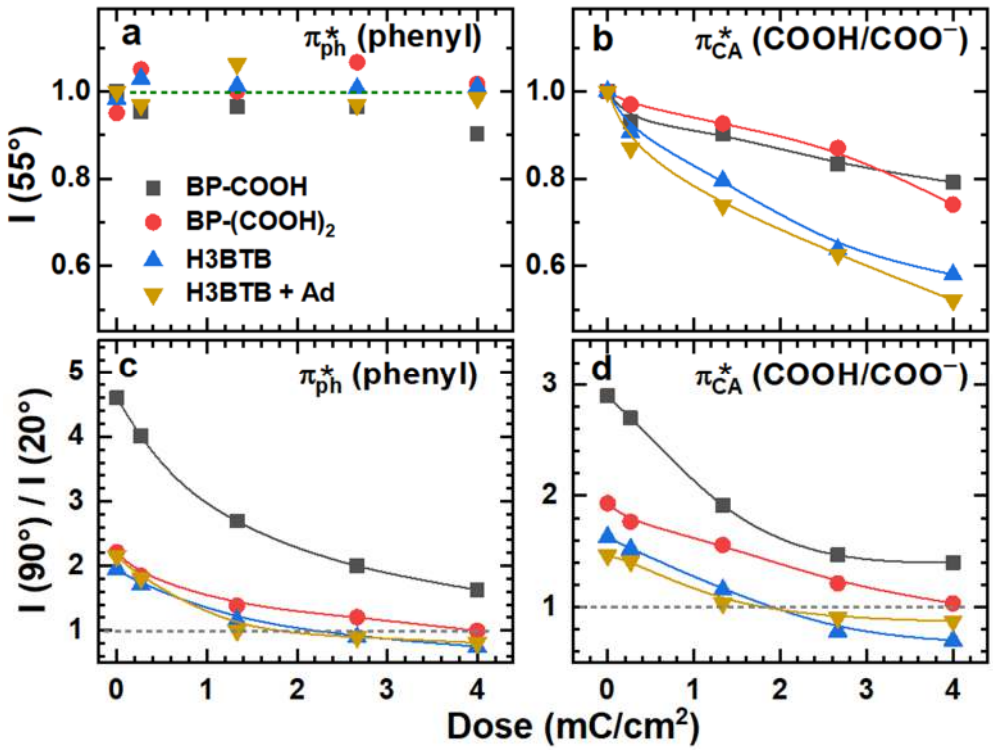

Figure 6. Intensities of the π^*_{ph} (a) and π^*_{CA} (b) resonances in the 55° NEXAFS spectra of the CA-based SAMs, and the respective I(90°)/I(20°) intensity ratios (c, d) as functions of irradiation dose. For legend to symbols see panel a. Solid lines are guides to the eye. The accuracy of the experimental values is ±5%.

Turning now to the NEXAFS data shown in Figure 6, they provide complementary structural information. Note that, in contrast to the XPS-derived parameters reflecting the evolution of the absolute values, the intensities of the NEXAFS resonances reflect relative values due to the normalization of the spectra (Figures 2c and 3c) to the entire amount of the respective atoms. Consequently, the approximately constant π^*_{ph} resonance intensity (Figure 6a) and progressively decreasing π^*_{CA} resonance intensity (Figure 6b) reflect the predominant damage/modification of the CA groups as compared to the aromatic backbone. The π^*_{CA} resonance intensity for the BP-CA and BP-dCA SAMs show nearly identical behavior in spite of double the number of the CA groups in the latter case. However, the π^*_{CA} signal for the BP-dCA SAM predominantly stems from the terminal CA group since that of the COO^- docking groups is strongly attenuated and comparably small. As far as the number of the terminal CA groups is doubled, which is the case for the H3BTB and H3BTB/Ad-CA monolayers, the drop of the π^*_{CA} signal upon irradiation becomes nearly twice that high (Figure 6b). Thus, the data in Figure 6b agree well with those in Figure 5c.

Finally, assessing the effects of electron irradiation on the molecular orientation and order in the SAMs, we look at the dose dependent ratio of the resonance intensities of the 90° and 20° NEXAFS spectra (Figures 6d and 6c). Similar to the difference spectra presented above (Figures 2d and 3d), the intensity ratio I(90°)/I(20°) represents a convenient indicator to trace structural changes, with random orientation of the planes of the aromatic rings or the CA groups reflected by a value of 1. Deviations to larger/smaller values indicate a progressively more upright/flat orientation. For the ratio values around one it is important to realize that there is an inherent ambiguity in the interpretation as it can either mean a wide and ultimately random distribution of orientations, a narrow distribution around a value of 54.7°, the so-called magic angle, or an average of well defined but distinctly different values such as the combination of upright orientated and flat-lying moieties.

The behavior of the intensity ratios in Figures 6d and 6c reflect a progressive disordering in the case of the BP-CA and BP-dCA SAMs which, in view of the initially small inclination of the molecules, is especially well pronounced in the case of the BP-CA monolayer. However, the course of the data indicates a residual alignment which cannot be concluded for BP-dCA as the ratio approaches the value of one. For the H3BTB and H3BTB/Ad-CA monolayers also a decrease in the ratio is observed. However, the crucial difference to the other systems is that the ratio does not level off at one but becomes distinctly lower, manifesting reorientation opposite to disordering as will be further discussed in Sec. 4. The average tilt angle of the

transition dipole moment (TDM) of the π^*_{ph} orbitals with respect to the surface normal in both H3BTB and H3BTB/Ad-CA monolayers was determined to ~49° at a dose of 4 mC/cm^2 which corresponds to a change by ~20° compared to the pristine SAMs and the TDM of the π^*_{CA} orbitals exhibited the similar behavior. Note, however, that the extent of the reorientation is presumably even larger, since it is certainly accompanied by general disordering of the monolayer - a typical behavior of SAMs under electron irradiation - tending to the elimination of the linear dichroism and, consequently, to a diminishing of the molecular reorientation effect in the NEXAFS spectra. Note also that since the π* orbitals are perpendicular to the planes of the phenyl rings and CA groups, the molecular tilt cannot be easily obtained from the orientation of the respective TDMs, since it is not only affected by tilt of the respective building blocks but by their twist as well.[69]

3.4. STM Data for the H3BTB SAM

In general, the well defined crystalline structure of SAMs is lost upon electron irradiation due to reorientation processes associated with the desorption of molecules and fragments, and the formation of an amorphous network of cross-linked molecules.[18,19] Usually monitored by spectroscopy as presented above, high resolution scanning probe techniques have rarely been employed to obtain structural information[44,70] as imaging of disordered structures is challenging and the information obtained is somewhat limited as regards the level of detail. However, since changes in the H3BTB-based SAMs observed by NEXAFS spectroscopy suggest some reorientation of the molecules and not just an amorphization of the layer, we endeavoured to use STM to see how the H3BTB SAM structure evolves with electron irradiation.

Representative STM data for the pristine and irradiated (1 mC/cm^2) H3BTB SAMs are presented in Figure 7. STM images for higher doses of 3 and 10 mC/cm^2 can be found in the Supporting Information (Figure S3). The STM image and height profiles of the pristine H3BTB SAM in Figure 7a reflect the established[10,15] row structure of this monolayer, with an intrarow periodicity of ~3.6 Å and an interrow spacing of ~16 Å. The rows are comprised of the π-stacked H3BTB molecules, while the entire structure is further stabilized by hydrogen bonding interactions between the terminal COOH groups of adjacent rows.

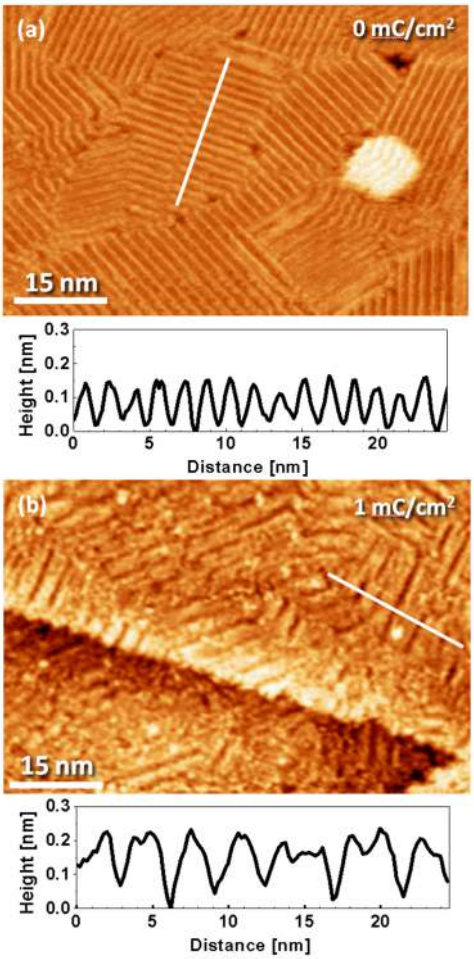

Figure 7. STM images (*ex situ*) and representative apparent height profiles for the pristine (a) and irradiated (1 mC/cm^2; b) H3BTB SAMs. The height profiles were measured along the white lines shown in the images.

Irradiation with a rather low dose of 1 mC/cm^2 (Figure 7b) already triggers substantial changes in the layer. While a domain structure can still be seen, the highly periodic row structure of the pristine SAM is changed into another less regular one whose most obvious features are a larger corrugation and the appearance of grooves which exhibit a wider and less regular separation compared to the rows of the pristine layer. A closer look reveals that, as illustrated by the left and right halves of the line profile of Figure 7b, the grooves are frequently separated twice or three times the row distance observed in the pristine layer. The observation of these aligned grooves strongly suggests that there still is a significant degree of long-range order in the monolayer, which supports the interpretation of the NEXAFS data (Figure 6d) that the ratio value close to one is not an amorphization of the layer but the result of a molecular reorientation. We note at this point that, in contrast to the pristine layer, no molecular resolution was obtained for the irradiated samples. However, this leaves open

whether this is a loss of regularity along the grooves or whether this an imaging issue as high resolution and stable imaging becomes progressively more difficult with increasing dose. Since imaging was performed in ambient environment after a few days storage of the samples (see Sec. 2) we explain this by the samples becoming more prone to contamination due to the structural and chemical changes of the SAM upon irradiation.[71] Nevertheless images of samples irradiated at higher doses of 3 and 10 mC/cm^2 (Figure S3 in the Supporting Information) suggest that the grooves disappear leading to the conclusion that the irradiation-induced molecular reorientation, traced by the NEXAFS spectroscopy, relies on short-range ordered structures. We will return to this point in Sec. 4

3.5. Higher Doses

Along with the extensive experiments performed for the entire series of the CA-based SAMs over a range of low irradiation doses, we carried out control experiments on the H3BTB monolayer over a broad range of doses using a different experimental setup (see Sec. 2 for details). Representative O 1s XP spectra can be found in the Supporting Information (Figure S4). The behavior of the total O 1s intensity is presented in Figure 8 for both sets of data. In spite of different equipment used for their acquisition, the data of both series correlate nicely with each other, representing the behavior for both low and high doses. Underlining the reproducibility of our experiments and data evaluation procedure, the extended range data are of importance on their own as they show that at high doses the CA signal levels off at about 20% of the intensity of the pristine layer, i.e., it is strongly reduced but does not disappear completely. Interestingly, the experimental data in Figure 8 could not be fitted by a single exponential function, as is frequently observed for irradiation-induced processes (see e.g. refs. [18] or [68]), but required a biexponential function. This means that the irradiation-induced damage and modification of the CA groups are complex processes with probably varying reaction pathways and restructuring processes in the course of the electron exposure. We note that the carboxylate component of the O 1s signal exhibits the same course as the COOH signal, i.e., also levels off. This is in contrast to the BP2-CA SAM for which a nearly complete disappearance of the O 1s signal at a dose of 150 mC/cm^2 is observed.[16] The obvious difference between the two molecules is that the carboxylate moiety is directly attached to an aromatic system in BP-CA but to an aliphatic linker in the case of BP2-CA. Since aliphatic chains are prone to decomposition rather than cross-linking, e.g. exhibit positive resist behaviour, we speculate that the different linkage of the carboxylate to the biphenyl unit gives rise to the difference.

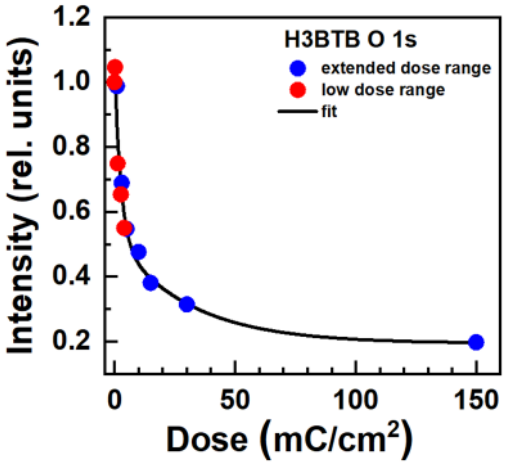

Figure 8. Total O 1s intensity for the H3BTB SAM as a functions of irradiation dose. The signal is the sum of contributions from all components (COO^-, C=O, and C–OH). The values are normalized to the intensity of the pristine SAM. Two sets of data are shown, acquired with different experimental setups and covering different dose ranges. The behavior of the experimental points is reproduced by a biexponential fit with decay constants of 0.39 and 0.032 cm^2/C. The accuracy of the experimental values is ±5%.

3.6. Electrochemical Deposition of Cu

To visualize the effect of electron irradiation and to prove the efficiency of cross-linking for aromatic molecules with Y-shape geometry, we performed the electrochemical deposition of Cu on an H3BTB-based template, patterned in proximity printing geometry (see Sec. 2 for technical details). A schematic of the patterning and electrodeposition procedure is shown in Figure 9a. As far as efficient cross-linking of a SAM takes place, irradiated areas are rendered electrochemically passive,[40,72] thus limiting the deposition of Cu to the non-irradiated areas and yielding a pattern which replicates the mesh structure of the mask. This is indeed the case for the patterned H3BTB SAM, as demonstrated in Figure 9b showing an AFM image of the sample after the electrochemical deposition of Cu. The fabricated pattern establishes that H3BTB behaves as negative resist like other aromatic SAMs. Notably, it shows a high contrast, with no Cu deposition within the irradiated areas (dark circular areas in image), and extensive Cu deposition within the non-irradiated areas. This contrast is further emphasized by the height profile across the fabricated pattern in Figure 9c, showing a thickness of the deposited Cu pattern of 45-50 nm for this sample. Noting that since the SAM-templated electrodeposition is sensitive to defects, such a high contrast is only possible if cross-linking is very efficient, thus eliminating point defects which can act as nucleation centers in the deposition process. Considering the open structure of an H3BTB SAM this result is

interesting as it extends the flexibility in the design of SAMs as electron beam resist materials beyond rod-like or disc-shaped molecules.[44]

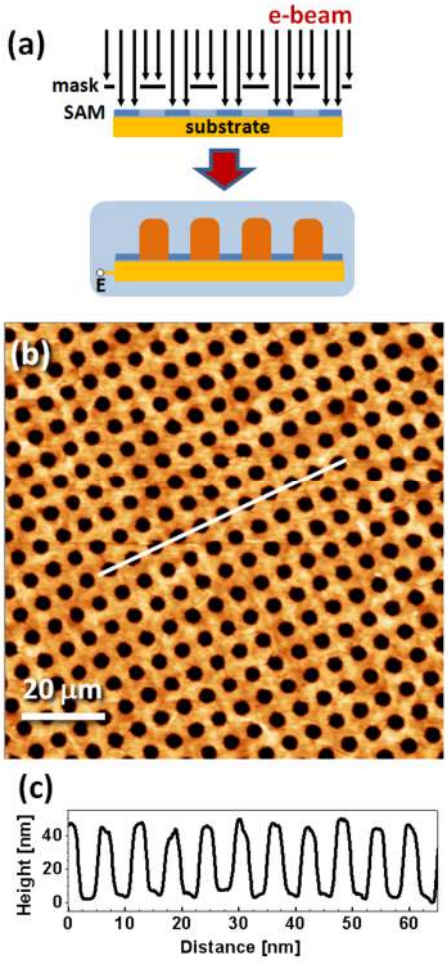

Figure 9. (a) Scheme of proximity patterning of a SAM by electron irradiation through a mask and the subsequent electrochemical deposition of Cu on the resulting template; (b) AFM image of a H3BTB SAM patterned with a dose of ~100 mC/cm^2 and taken after the deposition, and (c) height profile along the white line in the image. In (a), the areas exposed and not exposed to electrons are shown in dark and light blue, respectively.

4. Discussion

Whereas some interpretation of the irradiation-induced modification of the SAMs has already been presented along with the experimental data, we would like to focus in this section on the discussion of a few specific aspects. First, some of the irradiation-induced changes seem to be general features of CA-based aromatic SAMs, not only shared by the different SAMs investigated here but being also characteristic of BP2-CA/Ag[16] - a system structurally very similar to BP-CA. The most obvious ones are a substantial decrease in the carboxylate O 1s intensity (Figure 5b) and a significant reduction in the film thickness (Figure 5a). These

features pinpoint a distinct difference between CA and chalcogen-based SAMs. BP[46,68] and BP2[16] allowing for direct comparison, the thiol and selenolate SAMs show a noticeably smaller reduction in film thickness and drop in signal of the docking group upon electron irradiation than the CA SAMs. Hence, the Ch–M interface (Ch = S, Se; M = Au, Ag), more stable for Ag and less stable for Au,[18] is in any case much more robust against electron irradiation than the CA-Ag interface. The consequences are an extensive reduction (Figure 8) or even complete[16] elimination of the docking groups at high doses, thus resulting in the desorption of entire molecules and a comparably large thickness reduction (Figure 5a), which, however, occurs predominantly throughout the initial stage of the irradiation treatment, before the onset of extensive cross-linking.

Second, it is interesting to compare BP-CA with the closely related system BP2-CA reported in the literature.[16] The C 1s XP spectrum of the pristine BP-CA SAM, characterized by the single component of the carboxylate bidentate unit, develops a second component at about 1 eV higher BE which amounts to about 20% of the carboxylate signal at 4 mC/cm^2. Located at the BE of carbonyl oxygen it has the same narrow line width as the main signal (~1 eV) and no other components appear at higher binding energies. This is decisively different to BP2-CA where, at comparable dose, a multicomponent tail is observed whose integrated intensity adds up to a value in the range of the carboxylate signal.[16] These broad features are indicative of an irradiation-induced chemistry involving different pathways to form oxygen containing functional groups such as anhydrides, esters, or ketones which cover a wide range of BEs,[67] whereas BP-CA seems to invoke a more specific process. The simplest explanation, which is in full agreement with the experimental observations, is a change in the bonding configuration of the carboxylate moiety from bidentate to monodentate. Analogous to other systems,[73,74] the unbound oxygen atom will then exhibit a O 1s XP peak at a well defined BE, characteristic of carbonyl oxygen, whereas the peak associated with the substrate linked oxygen atom remains essentially unshifted and located in the region of the carboxylate bond. Since BP-CA forms a densely packed SAM, a change in the density should only be possible if there is enough free space to allow for the associated reorientation of the biphenyl units. Therefore, some molecules have to desorb first, in agreement with the XPS data where a substantial change in the film thickness occurs before the monodentate reaches detectable levels at doses somewhere between 1.35 and 2.7 mC/cm^2. The reorientation increases the disorder in the SAM as reflected by the dichroism of the π-resonances in the NEXAFS spectra. It is noted that, in contrast to the XP spectra which reflect the change in density, the 55° NEXAFS spectrum would not be significantly affected as the π^*_{CA} resonance is expected to appear at

the same energy.[75] As far as the difference between BP-CA and BP2-CA is concerned, it is reasonable to explain it by the absence/presence of the short aliphatic linker unit. This linker does change the general reaction of the given SAM to irradiation (similar behavior as for purely aromatic SAMs)[44,76] but can of course be of importance as far as the SAM/substrate interface is particular prone to irradiation-induced modification, which is the case for SAMs with CA docking group.

Third, beyond the trends common to all systems there are important quantitative and qualitative differences between them. For the compounds with terminal COOH groups the O 1s XP spectra (Figures 4 and 5d-f) exhibit clear differences in how the C–OH and C=O regions change in the initial stages of irradiation, thus, suggesting different mechanisms at work, i.e., the desorption of molecular entities and the chemistry involved in the cross-linking are substantially dependent on the details of the system.

Another obvious difference between the systems is the extent to which irradiation increases disorder and/or triggers reorientation of the molecules, reflected in the change of the I(90°)/ I(20°) ratios (Figure 6c,d). The systems can be divided into two sets, one consisting of SAMs of the homologous molecules of BP-CA and BP-dCA, the other one of the two H3BTB-based monolayers. Qualitatively, BP-CA and BP-dCA exhibit the same behaviour which is a substantial deterioration of the order reflected by the decrease of the I(90°)/I(20°) signals. There are some quantitative differences as the SAMs in their initial states differ in packing density and molecular orientation. BP-CA with a very upright orientation (~10° tilt of the molecular axis from the surface normal) exhibits a large change, yet within the dose range investigated some order persists resulting in an average tilt angle of ~27°. For BP-dCA, where molecules are more tilted and packed less dense (by ~10%) in the native SAM compared to BP-CA, there is no sign of residual order. While the course of the BP-CA data suggests that the disordering levels off due to progressing cross-linking in the layer it remains to be established by extending the dose range.

The second set of systems, the H3BTB-based SAMs, behave pronouncedly different as the course of the I(90°)/I(20°) ratio does not converge to one but changes from values >1 to <1 (Figure 6c,d). Even though disordering certainly contributes, the evolution of the I(90°)/I(20°) ratio, reflecting the orientation of the TDMs of the π^*_{ph} and π^*_{CA} orbitals, evidences the occurrence of distinctive reorientation processes. Accompanied by a continuous change in the orientation of individual building blocks, traced by the I(90°)/I(20°) ratio, this process must be related to the specific Y-shape of the H3BTB molecule and to an open structure of the

respective SAM, in contrast to the biphenyl-based monolayers, which form compact layers as illustrated in Figure 1. As a consequence, additional pathways for structural changes open up as, e.g., illustrated by the process outlined in Figure 10, which we consider a realistic scenario.

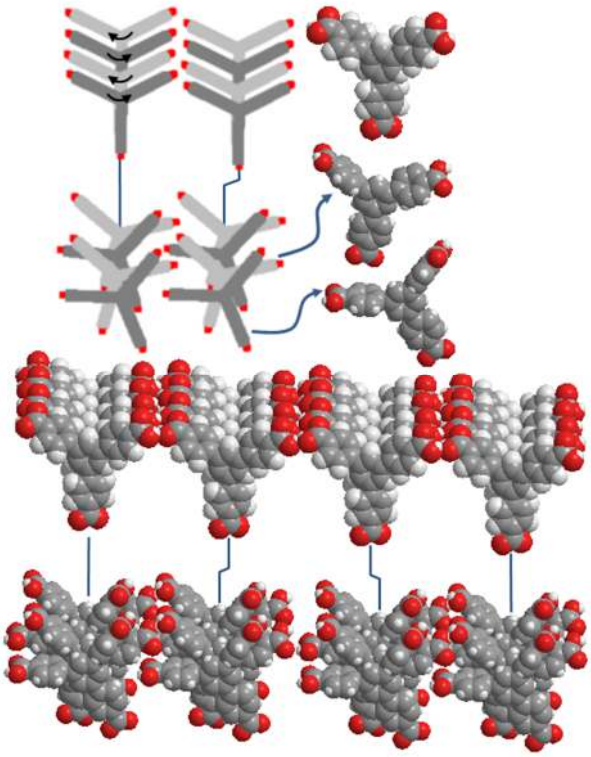

Figure 10. Schematic of the proposed radiation-induced rearrangements in a SAM of H3BTB. Top two rows illustrate changes in conformation when going from the eclipsed to a staggered arrangement. Bottom rows illustrate transition from the regular row structure of the native SAM to a row structure with variations in the row distance. For details see text.

In the native layer (top row in Figure 10) H3BTB arrange in very regular rows (see the STM image in Figure 7a), mediated by π-π and hydrogen bonding interactions. Due to the open structure of the SAM, there are some rotational degrees of freedom as schematically indicated in the second row in Figure 10. We note that (i) the regular alternating clockwise and counter-clockwise rotation of the molecules represents an idealized simplified scenario to illustrate the point and a less regular arrangement would probably be more realistic, and (ii) the changes are not necessarily static in nature. Compared to the eclipsed row structure, the staggered arrangement is energetically less favorable but the energy would come from the electron irradiation. Once molecules are in a staggered arrangement, there would be sufficient space

for them to afford conformational changes as illustrated by the space filling models in Figure 10. The terminal benzoic acid moieties can now rotate out of the molecular plane, thus creating sets of aromatic rings with very different orientations. This is seen from the comparison of the molecule in the native layer with the rotated ones where some of the terminal benzoic acid moieties are now orientated differently compared to the pristine SAMs, resulting in a substantial change in the average orientation of the TDMs of the π^*_{ph} and π^*_{CA} orbitals towards the surface normal, as observed experimentally (see Sec. 3.3).

There are some important points which follow from this behavior. First, a rotation would likely be paralleled by a change in density, i.e. film thickness, similar to BP-CA, as discussed above, but with the difference that it can occur from the beginning in parallel to desorption due to the open structure. Unfortunately, the spectral signature of the free COOH groups masks the changes associated with the anchoring configuration, thus impeding to gather direct spectroscopic evidence. To pinpoint this, experiments with SAMs of molecules geometrically analogous but with only one COOH group (e.g. 1,3-diphenyl-5-(4-carboxyphenyl)benzene or di(1H-pyrazol-1-yl)pyridine-4-yl)benzoic acid[11]) would be of interest. Second, the rotations of molecules and the subsequent changes create more space between the rows, which allows a reduction in distance between them (see models in bottom rows of Figure 10) and opening up a gap between other rows. Our observations of grooves, which are deeper and wider than in the original SAM and exhibit multiples of the original row periodicity (see Figure 7b), agree well with this model. Third, the more flat orientated aromatic units together with more free space available should facilitate the cross-linking. Since this process is associated with further changes in distance and orientation, any lateral azimuthal order is expected to be lost, in agreement with the STM images for the higher doses (Figure S3). However, a residual polar order would account for I(90°)/I(20°) ratio < 1. While we can explains our observations with this model, we stress its tentitativeness at this point and the need for further substantiation by more detailed experiments. Nevertheless, the obviously different behaviour of the conformationally flexible SAMs compared to densely packed ones consisting of rigid molecules offers additional options in the context of tailored cross-linking.

As the fourth and final aspect we would like to compare the H3BTB and H3BTB/Ad-CA SAMs which, as far as the overall arrangement of the H3BTB molecules is concerned, exhibit the same structure in the pristine state while the Ad-CA molecules are hidden in the nanotunnels formed by the H3BTB rows.[10,15] According to the experimental data, the H3BTB molecules in both the single-component and binary SAMs behave quite similarly upon the

exposure to electrons, including the irradiation-induced molecular reorientation (Figures 6c and 6d). The comparably small Ad-CA molecules do not disturb this behavior significantly but are themselves strongly prone to irradiation-induced desorption, resulting in a comparatively large loss of material (Figure 5a) and elimination of the COO^- docking groups (Figure 5b) as compared to the single-component H3BTB monolayer. Whereas the exact structure of the Ad-CA arrangement in the H3BTB nanotunnels is not known, one can assume that the intermolecular interaction in the arrangement, generally stabilizing a SAM in context of irradiation-induced damage,[76,77] is comparably weak. Along with the small size[78] and the sensitivity of the COO^- docking groups to irradiation (as shown in this work and ref. 16), this weakness is probably the reason for the particular proneness of the Ad-CA adlayer to irradiation-induced desorption. What remains open at this stage is how the Ad-CA affects the irradiation induced chemistry of H3BTB. The COOH range clearly exhibits differences over the whole range of doses studied as evidenced by Figures 4f,h and 5e,f but to what extent AdCA or its fragments are involved in the cross-linking chemistry or/and influence the orientational and conformational changes of the H3BTB molecules remains to be established.

5. Conclusions

Modification of aromatic CA-based SAMs by electron irradiation was studied comparing several representative systems which differ in molecular geometry, structure and functionalization. These systems comprised non-substituted and CA-substituted monolayers with the rod-like biphenyl backbone and SAMs of a Y-shaped, CA-substituted molecule, H3BTB, formed either as a single-component film or as a binary ordered monolayer by mixing with Ad-CA. With a focus on low irradiation doses, the SAMs showed not only surprisingly large changes in comparison to other types of monomolecular films but also distinct differences between them. The CA groups at both the SAM/substrate and SAM/ambient interface are prone to electron irradiation. However, in contrast to the CA groups at the outer SAM interface which are subject to substantial chemical changes as part of the cross-linking chemistry, the ones at the buried interface appear to be preserved but prone to configurational changes such as a transition from bidentate to monodentate. The latter bonding configuration is also considered as a possible intermediate state for molecular desorption which is the dominating process in the initial stage of irradiation until it is progressively hampered by the electron-induced cross-linking. The desorption processes are accompanied by pronounced changes in molecular orientation as pinpointed by NEXAFS spectroscopy with distinct differences between the biphenyl and H3BTB based systems. For

the densely packed biphenyl SAMs, molecular reorientation is synonymous with disordering, which is contrasted by the H3BTB monolayers where the progressive disordering is accompanied by molecular reorientation, so that at least a short-range orientational order is preserved to a significant extent. A model is proposed which explains this behavior by changes in molecular conformation afforded by the characteristic row structure of H3BTB SAM and the presence of nanotunnels.

The experiments presented here, in combination with the other two reports on cross-linked aromatic CA-SAMs,[16,17] indicate that this class of systems represents an interesting alternative to the established thiolate-based SAMs for lithography and nanofabrication. From the conceptual point of view, H3BTB is a particularly interesting example for two reasons. First, the results for this system suggest that a large conformational flexibility of SAM-forming molecules opens additional pathways for tailored cross-linking beyond the variation of rigid backbones used so far[44] and, thus, for control of properties such as membrane permeability or mechanical properties.[17,79] Second, the possibility of mixing molecules in a well-defined way, including the combination of aliphatic and aromatic components, further augments the opportunities for tuning the behavior of SAMs upon irradiation treatment, including the cross-linking chemistry and potential formation of structural motifs.

Associated content

Supporting Information

The Supporting Information is available free of charge on the ACS Publication website at DOI:
Additional spectroscopic and STM data (PDF).

Author Information

Corresponding Authors

*E-mail: mb45@st-andrews.ac.uk
*E-mail: Michael.Zharnikov@urz.uni-heidelberg.de

ORCID

Manfred Buck: 0000-0003-1225-7607
Michael Zharnikov: 0000-0002-3708-7571

Current address

§ Institute of Functional Interfaces, Karlsruhe Institute of Technology (KIT), Hermann-von-Helmholtz-Platz 1, 76344 Eggenstein-Leopoldshafen, Germany

Notes

The authors declare no competing financial interest.

Acknowledgements

We thank the Helmholtz Zentrum Berlin for the allocation of synchrotron radiation beamtime at BESSY II and A. Nefedov and Ch. Wöll for the technical cooperation during the experiments there. A.A. acknowledges the financial support by the DAAD-Aceh Scholarship of Excellence. Financial support by EPSRC via doctoral training grants (R.O.d.l.M.) and the EPSRC Centre for Doctoral Training in Critical Resource Catalysis (CRITICAT) (PhD studentship to K. T.) is gratefully acknowledged. We also thank S. Francis for technical support in setting up the irradiation chamber for patterning.

References

(1) Love, J. C.; Estroff, L. A.; Kriebel, J. K.; Nuzzo, R. G.; Whitesides, G. M. Self-Assembled Monolayers of Thiolates on Metals as a Form of Nanotechnology. *Chem. Rev.* **2005**, *105*, 1103–1169.

(2) Vericat, C.; Vela, M. E.; Benitez, G.; Carro, P.; Salvarezza, R. C. Self-Assembled Monolayers of Thiols and Dithiols on Gold: New Challenges for a Well-Known System. *Chem. Soc. Rev.* **2010**, *39*, 1805–1834.

(3) Tao, Y. T.; Lee, M. T.; Chang, S. C. Effect of Biphenyl and Naphthyl Groups on the Structure of Self-Assembled Monolayers - Packing, Orientation, and Wetting Properties. *J. Am. Chem. Soc.* **1993**, *115*, 9547-9555.

(4) Hsu, M. H.; Hu, W. S.; Lin, J. J.; Hsu, Y. J.; Wei, D. H.; Yang, C. W.; Chang, C. S.; Tao, Y. T. H_2S-Induced Reorganization of Mixed Monolayer of Carboxylic Derivatives on Silver Surface. *Langmuir* **2004**, *20*, 3641-3647.

(5) Cebula, I.; Lu, H.; Zharnikov, M.; Buck, M. Monolayers of Trimesic and Isophthalic Acid on Cu and Ag: The Influence of Coordination Strength on Adsorption Geometry. *Chem. Sci.* **2013**, *4*, 4455-4464.

(6) Aitchison, H.; Lu, H.; Zharnikov, M.; Buck, M. Monolayers of Biphenyl-3,4',5-tricarboxylic Acid Formed on Cu and Ag from Solution. *J. Phys. Chem. C* **2015**, *119*, 14114-14125.

(7) Aitchison, H.; Lu, H.; Hogan, S. W. L.; Früchtl, H.; Cebula, I.; Zharnikov, M.; Buck, M. Self-Assembled Monolayers of Oligophenylenecarboxylic Acids on Silver Formed at the Liquid-Solid Interface. *Langmuir* **2016**, *32*, 9397-9409.

(8) Skibinski, E. S.; Song, A. Q.; DeBenedetti, W. J. I.; Ortoll-Bloch, A. G.; Hines, M. A. Solution Deposition of Self-Assembled Benzoate Monolayers on Rutile (110): Effect of π-π Interactions on Monolayer Structure. *J. Phys. Chem. C* **2016**, *120*, 11581-11589.

(9) Krzykawska, A.; Ossowski, J.; Zaba, T.; Cyganik, P. Binding Groups for Highly Ordered SAM Formation: Carboxylic versus Thiol. *Chem. Commun.* **2017**, *53*, 5748-5751.

(10) Aitchison, H.; Lu, H.; de la Morena, R. O.; Cebula, I.; Zharnikov, M.; Buck, M. Self-Assembly of 1,3,5-Benzenetribenzoic Acid on Ag and Cu at the Liquid/Solid Interface. *Phys. Chem. Chem. Phys.* **2018**, *20*, 2731-2740.

(11) Aitchison, H.; de la Morena, R. O.; Peifer, R.; Omar, S.; Lu, H.; Francis, S. M.; Zharnikov, M.; Grohmann, A.; Buck, M. Self-Assembly of Di(pyrazol-1-yl)pyridine-benzoic Acid on Underpotentially Deposited Ag from Solution. *Langmuir* **2018**, *34*, 9654-9664.

(12) Krzykawska, A.; Szwed, M.; Ossowski, J.; Cyganik, P. Odd–Even Effect in Molecular Packing of Self-Assembled Monolayers of Biphenyl-Substituted Fatty Acid on Ag(111). *J. Phys. Chem. C* **2018**, *122*, 919-928.

(13) Johnson, K. N.; Hurlock, M. J.; Zhang, Q.; Hipps, K. W.; Mazur, U. Balancing Noncovalent Interactions in the Self-Assembly of Nonplanar Aromatic Carboxylic Acid MOF Linkers at the Solution/Solid Interface: HOPG vs Au(111). *Langmuir* **2019**, *35*, 5271-5280.

(14) DeBenedetti, W. J. I.; Hines, M. A. Breaking π-π Interactions in Carboxylic Acid Monolayers on Rutile TiO_2(110) Leads to Unexpected Long-Range Ordering. *J. Phys. Chem. C* **2019**, *123*, 8836-8842.

(15) de la Morena, R. O.; Asyuda, A.; Lu, H.; Aitchison, H.; Turner, K.; Francis, S. M.; Zharnikov, M.; Buck, M. Shape Controlled Assembly of Carboxylic Acids: Formation of a Binary Monolayer by Intercalation into Molecular Nanotunnels. *Phys. Chem. Chem. Phys.* **2020**, *22*, 4205-4215.

(16) Neumann, C.; Szwed, M.; Frey, M.; Tang, Z.; Kozieł, K.; Cyganik, P.; Turchanin, A. Preparation of Carbon Nanomembranes without Chemically Active Groups, *ACS Appl. Mater. Interfaces* **2019**, *11*, 31176−31181.

(17) Dementyev, P.; Naberezhnyi, D.; Westphal, M.; Buck, M.; Gölzhäuser, A. Carbon Nanomembranes from Aromatic Carboxylate Precursors. *ChemPhysChem* **2020**, *21*, 1006-1011.

(18) Zharnikov, M.; Grunze, M. Modification of Thiol-Derived Self-Assembling Monolayers by Electron and X-ray Irradiation: Scientific and Lithographic Aspects**.** *J. Vac. Sci. Technol. B* **2002**, *20*, 1793-1807.

(19) Turchanin, A.; Käfer, D.; El-Desawy, M.; Wöll, C.; Witte, G.; Gölzhäuser, A. Molecular Mechanisms of Electron-Induced Cross-Linking in Aromatic SAMs. *Langmuir* **2009**, *25*, 7342-7352.

(20) Zharnikov, M. High-Resolution X-Ray Photoelectron Spectroscopy in Studies of Self-Assembled Organic Monolayer. *J. Electron Spectr. Relat. Phenom.* **2010**, *178-179*, 380-393.

(21) Ballav, N.; Weidner, T.; Rößler, K.; Lang, H.; Zharnikov, M. A New Approach for the Fabrication of Strongly Heterogeneous Mixed Self-Assembled Monolayers. ChemPhysChem **2007**, *8*, 819 – 822.

(22) Jeyachandran, Y. L.; Zharnikov, M. A Comprehensive Analysis of the Effect of Electron Irradiation on Oligo(ethylene glycol) Terminated Self-Assembled Monolayers Applicable for Specific and Non-specific Patterning of Proteins. *J. Phys. Chem. C* **2012**, *116*, 14950–14959.

(23) Ballav, N.; Shaporenko, A.; Terfort, A.; Zharnikov, M. A Flexible Approach to the Fabrication of Chemical Gradients. *Adv. Mat.* **2007**, *19*, 998–1000.

(24) Ballav, N.; Thomas, H.; Winkler, T.; Terfort, A.; Zharnikov, M. Making Protein Patterns by Writing in a Protein-Repelling Matrix. *Angew. Chem. Int. Ed.* **2009**, *48*, 5833-5836.

(25) Tai, Y.; Shaporenko, A.; Noda, H.; Grunze, M.; Zharnikov, M. Fabrication of a Stable Metal Film on the Surface of Self-Assembled Monolayers. *Adv. Mater.* **2005**, *17*, 1745 – 1749.

(26) Chesneau, F.; Terfort, A.; Zharnikov, M. Nickel Deposition on Fluorinated, Aromatic Self-Assembled Monolayers: Chemically Induced Cross-Linking as a Tool for the Preparation of Well-Defined Top Metal Films. *J. Phys. Chem. C* **2014**, *118*, 11763−11773.

(27) Sauter, E.; Yildirim, C.; Terfort, A.; Zharnikov, M. Adjustment of the Work Function of Pyridine and Pyrimidine Substituted Aromatic Self-Assembled Monolayers by Electron Irradiation. *J. Phys. Chem. C* **2017**, *121*, 12834–12841.

(28) Geyer, W.; Stadler, V.; Eck, W.; Zharnikov, M.; Gölzhäuser, A.; Grunze, M. Electron Induced Cross-Linking of Aromatic Self-Assembled Monolayers: Negative Resists for Nanolithography. *Appl. Phys. Lett.* **1999**, *75*, 2401-2403.

(29) Eck, W.; Stadler, V.; Geyer, W.; Zharnikov, M.; Gölzhäuser, A.; Grunze, M. Generation of Surface Amino Groups on Aromatic Self-Assembled Monolayers by Low Energy Electron Beams - A First Step Towards Chemical Lithography. *Adv. Mater.* **2000**, *12*, 805-808.

(30) Gölzhäuser, A.; Geyer, W.; Stadler, V.; Eck, W.; Grunze, M.; Edinger, K.; Weimann, Th.; Hinze. P. Nanoscale Patterning of Self-Assembled Monolayers with Electrons. *J. Vac. Sci. Technol. B* **2000**, *18*, 3414-3418.

(31) Gölzhäuser, A.; Eck, W.; Geyer, W.; Stadler, V.; Weimann, T.; Hinze, P.; Grunze, M. Chemical Nanolithography with Electron Beams. *Adv. Mater.* **2001**, *13*, 803-806.

(32) Schmelmer, U.; Jordan, R.; Geyer, W.; Eck, W.; Gölzhäuser, A.; Grunze, M.; Ulman, A. Surface-Initiated Polymerization on Self-Assembled Monolayers: Amplification of Patterns on the Micrometer and Nanometer Scale. *Angew. Chem. Int. Ed.* **2003**, *42*, 559-563.

(33) Gates, B. D.; Xu, Q.; Stewart, M.; Ryan, D.; Willson, C. G.; Whitesides, G. M. New Approaches to Nanofabrication: Molding, Printing, and Other Techniques. *Chem. Rev.* **2005**, *105*, 1171-1196.

(34) Turchanin, A.; Tinazli, A.; El-Desawy, M.; Grossann, H.; Schnietz, M.; Solak, H. H.; Tampe, R.; Gölzhäuser, A. Molecular Selfassembly, Chemical Lithography, and Biochemical

Tweezers: A Path for the Fabrication of Functional Nanometer-Scale Protein Arrays. *Adv. Mater.* **2008**, *20*, 471−477.

(35) Shah, S. S.; Howland, M. C.; Chen, Li-J.; Silangcruz, J.; Verkhoturov, S. V.; Schweikert, E. A.; Parikh, A. N.; Revzin, A. Micropatterning of Proteins and Mammalian Cells on Indium Tin Oxide. *ACS Appl. Mater. Interfaces* **2009**, *1*, 2592–2601.

(36) Saavedra, H. M.; Mullen, T. J.; Zhang, P.; Dewey, D. C.; Claridge, S. A.; Weiss, P. S. Hybrid Strategies in Nanolithography. *Rep. Prog. Phys.* **2010**, *73*, 036501.

(37) Shestopalov, A. A.; Clark, R. L.; Toone, E. J. Inkless Microcontact Printing on SAMs of Bocand TBS-Protected Thiols. *Nano Lett.* **2010**, *10*, 43-46.

(38) Turchanin, A.; Gölzhäuser, A. Carbon Nanomembranes from Self-Assembled Monolayers: Functional Surfaces Without Bulk. *Prog. Surf. Sci.* **2012**, *87*, 108-162.

(39) Khan, M. N.; Tjong, V.; Chilkoti, A.; Zharnikov, M. Fabrication of ssDNA/Oligo(ethylene glycol) Monolayers and Complex Nanostructures by an Irradiation-Promoted Exchange Reaction. *Angew. Chem. Int. Ed.* **2012**, *51*, 10303–10306.

(40) She, Z.; DiFalco, A.; Hähner, G.; Buck, M. Electron-Beam Patterned Self-Assembled Monolayers as Templates for Cu Electrodeposition and Lift-Off. *Beilst. J. Nanotechnol.* **2012**, *3*, 101-113.

(41) Eck, W.; Küller, A.; Grunze, M.; Völkel, B.; Gölzhäuser, A. Freestanding Nanosheets from Crosslinked Biphenyl Self-Assembled Monolayers. *Adv. Mater.* **2005**, *17*, 2583−2586.

(42) Zheng, Z.; Nottbohm, C. T.; Turchanin, A.; Muzik, H.; Beyer, A.; Heilemann, M.; Sauer, M.; Gölzhäuser, A. Janus Nanomembranes: A Generic Platform for Chemistry in Two Dimensions. *Angew. Chem. Int. Ed.* **2010**, *49*, 8493 –8497.

(43) Meyerbröker, N.; Li, Zi-An; Eck, W.; Zharnikov, M. Biocompatible Nanomembranes Based on PEGylation of Cross-Linked Self-Assembled Monolayers. *Chem. Mater.* **2012**, *24*, 2965–2972.

(44) Angelova, P.; Vieker, H.; Weber, N.-E.; Matei, D.; Reimer, O.; Meier, I.; Kurasch, S.; Biskupek, J.; Lorbach, D.; Wunderlich, K.; et al. A Universal Scheme to Convert Aromatic Molecular Monolayers into Functional Carbon Nanomembranes. *ACS Nano* **2013**, *7*, 6489–6497.

(45) Turchanin, A.; Gölzhäuser, A. Carbon Nanomembranes. *Adv. Mater.* **2016**, *28*, 6075–6103.

(46) Yildirim, C.; Füser, M.; Terfort, A.; Zharnikov, M. Modification of Aromatic Self-Assembled Monolayers by Electron Irradiation: Basic Processes and Related Applications. *J. Phys. Chem. C* **2017**, *121*, 567–576.

(47) Neumann, C.; Wilhelm, R.; Küllmer, M.; Turchanin, A. Low-Energy Electron Irradiation Induced Synthesis of Molecular Nanosheets: An Influence of the Electron Beam Energy. *Faraday Discuss.* **2020**, DOI: 10.1039/C9FD00119K.

(48) Ballav, N.; Zharnikov, M. Reorientation Promoted Exchange Reaction in Aromatic Self-Assembled Monolayers. *J. Phys. Chem. C* **2008**, *112*, 15037-15044.

(49) Olsen, C.; Rowntree, P. A. Bond-Selective Dissociation of Alkanethiol Based Self-Assembled Monolayers Adsorbed on Gold Substrates, Using Low-Energy Electron Beams. *J. Chem. Phys.* **1998**, *108*, 3750-3764.

(50) Huels, M. A.; Dugal, P. C.; Sanche, L. Degradation of Functionalized Alkanethiolate Monolayers by 0–18 eV Electrons. *J. Chem. Phys.* **2003**, *118*, 11168-11178.

(51) Amiaud, L.; Houplin, J.; Bourdier, M.; Humblot, V.; Azria, R.; Pradier, C.-M.; Lafosse, A. Low-Energy Electron Induced Resonant Loss of Aromaticity: Consequences on Cross-Linking in Terphenylthiol SAMs. *Phys. Chem. Chem. Phys.* **2014**, *16*, 1050-1059.

(52) Schmid, M.; Wan, X.; Asyuda, A.; Zharnikov, M. Modification of self-assembled monolayers by electron irradiation: The effect of primary energy (10 - 500 eV). *J. Phys. Chem. C* **2019**, *123*, 28301−28309.

(53) Nefedov, A. Wöll, C. Advanced Applications of NEXAFS Spectroscopy for Functionalized Surfaces, in *Surface Science Techniques*; Bracco, G.; Holst, B., Eds.; Springer Series in Surface Science **2013**, *51*, 277-306; Springer-Verlag: Berlin, Heidelberg, New York, Tokyo.

(54) Moulder, J. F.; Stickle, W. E.; Sobol, P. E.; Bomben, K. D. *Handbook of X-ray Photoelectron Spectroscopy*, Chastian, J., Ed.; Perkin-Elmer Corp.: Eden Prairie, MN, 1992.

(55) Thome, J.; Himmelhaus, M.; Zharnikov, M.; Grunze, M. Increased Lateral Density in Alkanethiolate Films on Gold by Mercury Adsorption. *Langmuir* **1998**, *14*, 7435–7449.

(56) Ratner, M.; Castner, D. Electron Spectroscopy for Chemical Analysis, in *Surface Analysis - The principal techniques*; Vickerman, J. Ed.; Wiley: Chichester, 1997.

(57) Lamont, C. L. A.; J. Wilkes, Attenuation Length of Electrons in Self-Assembled Monolayers of *n*-Alkanethiols on Gold. *Langmuir* 1999, **15**, 2037-2042.

(58) Stöhr, J. *NEXAFS spectroscopy*; Springer-Verlag: Berlin, 1992.

(59) Batson, P. E. Carbon-1s Near-Edge-Absorption Fine-Structure in Graphite. *Phys. Rev. B* **1993**, *48*, 2608-2610.

(60) Horsley, J.; Stöhr, J.; Hitchcock, A. P.; Newbury, D. C.; Johnson, A. L.; Sette, F. Resonances in the K Shell Excitation Spectra of Benzene and Pyridine: Gas Phase, Solid, and Chemisorbed States. *J. Chem. Phys.* **1985**, *83*, 6099-6107.

(61) Yokoyama, T.; Seki, K.; Morisada, I.; Edamatsu, K.; Ohta, T. X-Ray Absorption Spectra of Poly-p-Phenylenes and Polyacenes: Localization of π* Orbitals. *Phys. Scr.* **1990**, *41*, 189-192.

(62) Zharnikov, M.; Kuller, A.; Shaporenko, A.; Schmidt, E.; Eck, W. Aromatic Self-Assembled Monolayers on Hydrogenated Silicon. *Langmuir* **2003**, *19*, 4682-4687.

(63) Zharnikov, M.; Frey, S.; Heister, K.; Grunze, M. An extension of the mean free path approach to X-ray absorption spectroscopy. *J. Electron Spectrosc. Relat. Phenom.* **2002**, *124*, 15-24.

(64) Ge, Y.; Weidner, T.; Ahn, H.; Whitten, J. E.; Zharnikov, M. Energy level pinning in self-assembled alkanethiol monolayers, *J. Phys. Chem. C* **2009**, *113*, 4575–4583.

(65) Taucher, T. C.; Hehn, I.; Hofmann, O. T.; Zharnikov, M.; Zojer, E. Understanding Chemical versus Electrostatic Shifts in X-Ray Photoelectron Spectra of Organic Self-Assembled Monolayers. *J. Phys. Chem. C* **2016**, *120*, 3428–3437.

(66) Houplin, J.; Amiaud, L.; Humblot, V.; Martin, I.; Matar, E.; Azria, R.; Pradier, C. M.; Lafosse, A. Selective Terminal Function Modification of SAMs Driven by Low-Energy Electrons (0-15 eV). *Phys. Chem. Chem. Phys.* **2013**, *15*, 7220-7227.

(67) Beamson, G.; Briggs, D. *High Resolution XPS of Organic Polymers.* Wiley-WCH: Weinheim, 1992.

(68) Weidner, T.; Ballav, N.; Grunze, M.; Terfort, A.; Zharnikov, M. Modification of Biphenylselenolate Monolayers by Low-Energy Electrons. *Phys. Stat. Sol.* **2009**, *246*, 1519–1528.

(69) Ballav, N.; Schüpbach, B.; Dethloff, O.; Feulner, P.; Terfort, A.; Zharnikov, M. Direct Probing Molecular Twist and Tilt in Aromatic Self-Assembled Monolayers. *J. Am. Chem. Soc.* **2007**, *129*, 15416–15417.

(70) Yang, Y.; Dementyev, P.; Biere, N.; Emmrich, D.; Stohmann, P.; Korzetz, R.; Zhang, X. H.; Beyer, A.; Koch, S.; Anselmetti, D.; Gölzhäuser, A. Rapid Water Permeation Through Carbon Nanomembranes with Sub-Nanometer Channels. *ACS Nano* **2018**, *12*, 4695-4701.

(71) Chen, C.-H.; Huang, M.-L.; Wang, S.-C.; Klauser, R.; Shaporenko, A.; Zharnikov, M. Exposure of Monomolecular Lithographic Patterns to Ambient: An X-ray Photoemission Spectromicroscopy Study. *J. Phys. Chem. B* **2006**, *110,* 17878-17883.

(72) Felgenhauer, T.; Yan, C.; Geyer, W.; Rong, H. T.; Gölzhäuser, A.; Buck, M. Electrode Modification by Electron-Induced Patterning of Aromatic Self-Assembled Monolayers. *Appl. Phys. Lett.* **2001**, *79*, 3323-3325.

(73) Dubois, L. H.; Zegarski, B. R.; Nuzzo, R. G. Spontaneous Organization of Carboxylic Acid Monolayer Films in Ultrahigh Vacuum. Kinetic Constraints to Assembly via Gas-Phase Adsorption. *Langmuir* **1986**, *2*, 412-417.

(74) Hwang, H.-N.; Baik, J. Y.; An, K.-S.; Lee, S. S.; Kim, Y.; Hwang, C. C.; Kim, B. Selectivity of the Chemisorption of Vinylacetic Acid on the Si(001)2×1 Surface. *J. Phys. Chem. B* **2004**, *108*, 8379-8384.

(75) Urquhart, S. G.; Ade, H. Trends in the Carbonyl Core (C 1S, O 1S) $\rightarrow \pi^*_{C=O}$ Transition in the Near-Edge X-ray Absorption Fine Structure Spectra of Organic Molecules. *J. Phys. Chem. B* **2002**, *106*, 8531-8538.

(76) Frey, S.; Rong, H.-T.; Heister, K.; Yang, Y.-J.; Buck, M.; Zharnikov, M. Response of Biphenyl-Substituted Alkanethiol Self-Assembled Monolayers to Electron Irradiation: Damage Suppression and Odd-Even Effects. *Langmuir* **2002**, *18*, 3142-3150.

(77) Cyganik, P.; Vandeweert, E.; Postawa, Z.; Bastiaansen, J.; Vervaecke, F.; Lievens, P.; Silverans, R. E.; Winograd. N. Modification and Stability of Aromatic Self-Assembled Monolayers upon Irradiation with Energetic Particles. *J. Phys. Chem. B* **2005**, *109*, 5085-5094.

(78) Hamoudi, H.; Chesneau, F.; Patze, C.; Zharnikov, M. Chain-Length-Dependent Branching of Irradiation-Induced Processes in Alkanethiolate Self-Assembled Monolayers. *J. Phys. Chem. C* **2011**, *115*, 534-541.

(79) Yang, Y.; Hillmann, R.; Qi, Y.; Korzetz, R.; Biere, N.; Emmrich, D.; Westphal, M.; Buker, B.; Hutten, A.; Beyer, A.; et al. Ultrahigh Ionic Exclusion through Carbon Nanomembranes. *Adv. Mater.* **2020**, *32*, 1907850.